

# Structural, electronic, and magnetic properties of Mn-doped Ge nanowires by *ab initio* calculations

J. T. Arantes, Antônio J. R. da Silva, and A. Fazzio

*Instituto de Física, Universidade de São Paulo,  
CP 66318, 05315-970 São Paulo, SP, Brazil*

(Dated: February 2, 2020)

## Abstract

Using *ab initio* total energy density-functional theory calculations, we investigate the electronic, structural and magnetic properties of Manganese doped Germanium nanowires. The nanowires have been constructed along the [110] direction and the dangling bonds on the surface have been saturated by hydrogen atoms. We observed that the Mn has lower formation energy at the center of the wire when compared to regions close to the surface. The Mn-Mn coupling has lower energy for a high-spin configuration except when they are first nearest neighbors. These results show that Ge:Mn nanowires are potential candidates for ferromagnetic quasi-one dimensional systems.

## I. INTRODUCTION

Semiconductor nanowires<sup>1</sup> are considered by many researchers as the class of nanomaterials that will become the major player in the future electronic technology. Among these nanowires, those composed by silicon (SiNWs) and germanium (GeNWs) have an intrinsic interest<sup>2,3</sup> because they may be more easily integrated with the current silicon-based technology. Besides the search for nanomaterials, a field that has attracted a great deal of attention due to possible developments of new devices is the study of diluted magnetic semiconductors (DMS)<sup>4,5</sup>. The DMS are usually composed by transition metals embedded in a semiconductor matrix, in a high enough concentration to render the material ferromagnetic below a certain critical temperature  $T_c$ . The highest critical temperatures so far achieved have been on III-V semiconductors. There is, however, a great interest in obtaining a DMS based on a type-IV semiconductor. Reports of ferromagnetism in  $Mn_xGe_{1-x}$  have been recently made<sup>6,7</sup>, as well as in Mn-implanted silicon<sup>8</sup>. There is an important difference between Mn doping in Si and Ge. A Mn impurity favors an interstitial site in Si, whereas in Ge it prefers a substitutional site<sup>9</sup>. As a consequence, a Mn substitutional in Ge cannot diffuse as easily as an interstitial Mn in Si<sup>10</sup>, allowing the introduction of a larger number of Mn in Ge without their diffusion and subsequent clustering.

Considering what has been described above, it seems relevant to study the behavior of Mn-doped Ge nanowires, and to investigate the effect of the quantum confinement on the properties of these DMS nanowires. The magnetic ordering in Mn-doped nanoparticles and nanowires semiconductors has been recently addressed by numerous investigations<sup>11,12,13</sup>. In particular, Libers group has obtained a general synthesis procedure of Mn-doped semiconductor nanowires<sup>14</sup>. These controlled processes to obtain nanowires doped with magnetic ions give us opportunities to understand the magnetic order in low-dimensional materials for future applications in spintronic nano-devices.

In this work we study, from theoretical point of view, the structural, electronic and magnetic properties of Mn doped GeNWs. In particular, we observe that the Mn has a lower formation energy at the center of the wire when compared to regions close to the surface. In the next section we describe the procedure we used in our calculations, followed by the section with the results and discussion. Finally, the main conclusions are summarized in the last section.

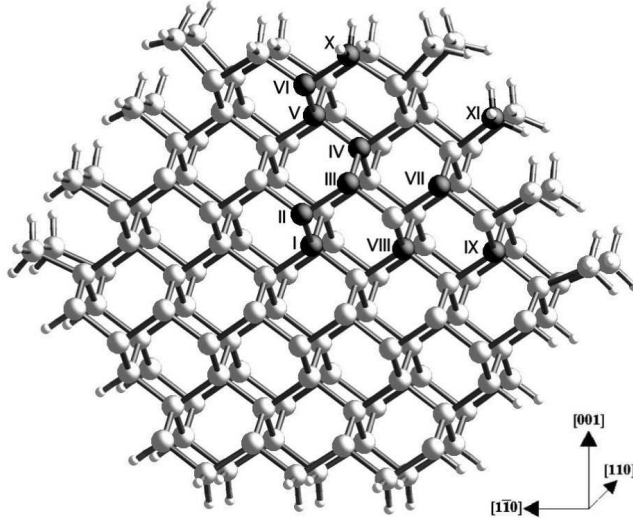


FIG. 1: Atomic geometry for the Ge nanowire with diameter  $d \simeq 27.0 \text{ \AA}$ . The larger gray spheres represent the Ge atoms and the small ones represent the hydrogen atoms at the surface. The black spheres represent the studied substitutional positions of the Mn impurity.

## II. CALCULATION PROCEDURE

All our results are obtained using total energy *ab initio* calculations based on spin-polarized density functional theory within the generalized gradient approximation (GGA)<sup>15</sup> for the exchange-correlation potential. We used ultrasoft pseudopotentials<sup>16</sup> and a plane wave expansion up to 230.0 eV, as implemented in the VASP code<sup>17</sup>. For bulk calculations we used 64 Ge atoms in a cubic supercell with a  $(3 \times 3 \times 3)$  Monkhorst-Pack Brillouin zone sampling. We studied four different NWs with zinc-blend structure grown along the  $[110]$  direction. The NW with diameter  $d \simeq 35.0 \text{ \AA}$  contains 322 atoms, with 218 Ge atoms and saturated by 104 H atoms. For the  $d \simeq 27.0 \text{ \AA}$  NW, used for most of our studies of Mn doping (figure 1), we have 214 atoms with 134 Ge and 80 H atoms. The diameter  $d \simeq 18.7 \text{ \AA}$  contains 116 atoms with 76 Ge and 40 H atoms. Finally, for the small diameter ( $d \simeq 14.7 \text{ \AA}$ ) the total number of atoms used was 60 with 36 Ge and 24 H atoms. For the nanowire calculations, we used a Brillouin zone sampling of three  $k$ -points corresponding to a  $(1 \times 1 \times 3)$  Monkhorst-Pack grid. In all calculations the positions of all atoms in the supercell were allowed to relax until all the forces were smaller than  $0.02 \text{ eV/\AA}$ . For all impurity calculations we have not fixed the value of the total spin of the supercell. In each case, however, we used as an initial guess a Mn high-spin configuration.

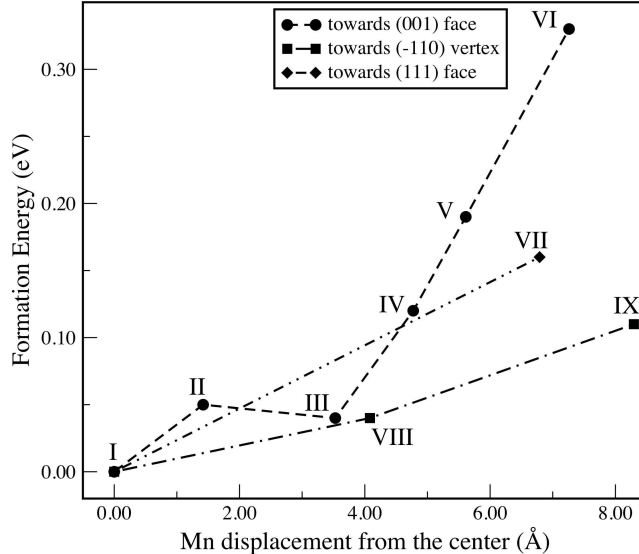


FIG. 2: Total energy for the substitutional Mn dopant sites in the Ge nanowires as a function of the dopant distance from the center of the nanowire. The reference zero energy is for the Mn in the center of the wire. The dashed lines are only guides to the eye, and they connect sites along paths towards either a particular face or a vertex.

### III. RESULTS AND DISCUSSIONS

All the GeNWs calculated with different diameters, as described below, have a hexagonal cross-section shape that exposes  $\{111\}$  and  $\{001\}$  faces (see figure 1). The corresponding angle between the exposed  $\{001\}$  and  $\{111\}$  ( $\{1\bar{1}1\}$ ) face is  $54.92^\circ$  ( $54.91^\circ$ ). The angle between the  $\{111\}$  face and the  $\{\bar{1}1\bar{1}\}$  face is  $70.74^\circ$ , in agreement with experimental results<sup>18</sup>. The average Ge-Ge bond length is  $2.49 \text{ \AA}$  close to the center of the wire and  $2.47 \text{ \AA}$  around the surface. The Ge-H bond length in the surface has an average of  $1.54 \text{ \AA}$ . For the pure nanowire, as expected, the band gap increases with the quantum confinement. The calculated band gaps are  $0.53$ ,  $0.78$ ,  $1.00$  and  $1.34 \text{ eV}$  for the diameters  $\simeq 35.0$ ,  $\simeq 27.0$ ,  $\simeq 18.7$ , and  $\simeq 14.7 \text{ \AA}$  respectively<sup>19</sup>.

In figure 2 we show our results for the substitutional Mn formation energy for the non-equivalent sites shown in figure 1. The energy reference is taken for the Mn substitutional in the center of the nanowire. The dashed lines are only guides to the eye, and they connect sites along paths towards either a particular face or a vertex. The formation energy,  $E_f^S$ , is

given by

$$E_f^S = (E_{def} + \mu_{Ge}) - E_{nw} - \mu_{Mn}, \quad (1)$$

where  $E_{def}$  is the total energy of the supercell with the Mn atom at a substitutional site and  $E_{nw}$  is the total energy of the nanowire without the Mn atom. The  $\mu_{Ge}$  and  $\mu_{Mn}$  are Ge and Mn chemical potentials, respectively. The results show that Mn has lower formation

TABLE I: The Mn-Ge bond length. The first column represents the labeled (I to XI) configurations of figure 1. In the second (third) column we show the longitudinal (cross-sectional) distances.

Config.	Long. distances (Å)	Cross distances (Å)
I	2.46, 2.46	2.48, 2.48
II	2.46, 2.46	2.48, 2.49
III	2.47, 2.46	2.48, 2.48
IV	2.45, 2.46	2.48, 2.48
V	2.44, 2.46	2.47, 2.47
VI	2.54, 2.49	2.46, 2.47
VII	2.47, 2.47	2.49, 2.49
VIII	2.46, 2.46	2.47, 2.48
IX	2.49, 2.48	2.46, 2.49
X	2.55	2.49, 2.52
XI	2.56	2.55

energy at the center of the Ge-nanowire.

In table I we show the distances between the Mn and its nearest neighbor Ge atoms for the sites labeled in figure 1. There are two types of neighbors and therefore two types of distances; the ones oriented along the direction of growth of the nanowire, which we will call longitudinal distances, and the ones oriented perpendicular to the growth direction, which we call cross-sectional distances. For Mn at the positions I to VIII, except position VI, there is a small distortion, presenting a slightly distorted local  $T_d$  symmetry. In all these configurations the Mn atom is surrounded by four Ge neighbors not bonded to saturating H-atoms. In general, the Mn nearest neighbors suffer a bond length decrease of 0.8% up to 1.6% when compared to a pure germanium nanowire. The position VI and IX present a

local  $C_{3v}$  symmetry. These positions are at sub-surface layers, allowing a larger relaxation for the Mn impurity.

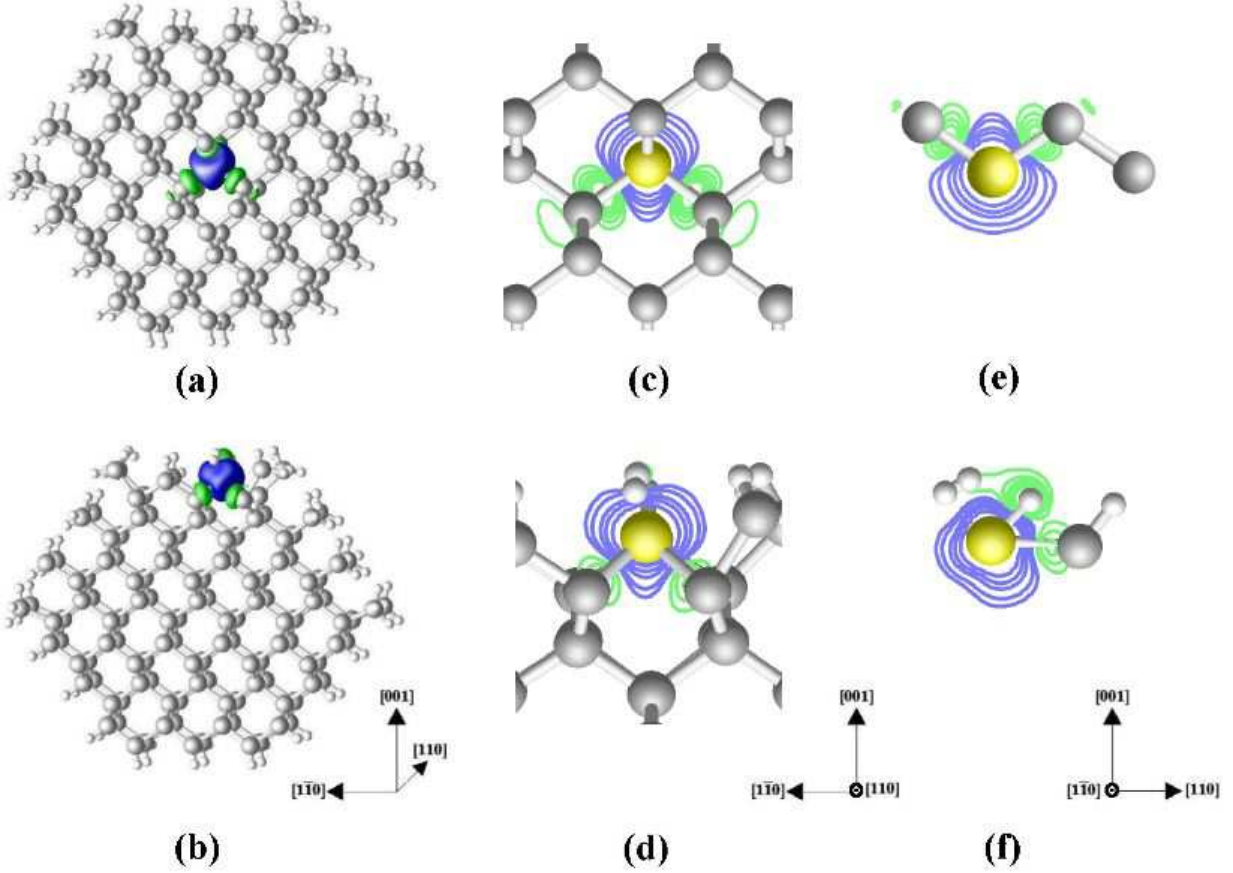


FIG. 3: (Color online) Isosurface for the net magnetization  $m(\mathbf{r}) = \rho_{up}(\mathbf{r}) - \rho_{down}(\mathbf{r})$  for a) Mn atom at position I, b) Mn atom at position X. Blue (green) regions represent predominant  $\rho_{up}$  ( $\rho_{down}$ ) electronic densities. The more spherical isosurfaces correspond to a net spin value of  $+0.01e/\text{\AA}^3$  and the four  $p$ -orbitals shaped isosurfaces correspond to a net spin value of  $-0.01e/\text{\AA}^3$ . In (c) and (d) we show the cross-sectional views and in (e) and (f) are the longitudinal views related to the isosurfaces depicted in (a) and (b). The outermost (innermost) green line has  $m(\mathbf{r}) = -0.01$  ( $m(\mathbf{r}) = -0.05$ ). The innermost (outermost) blue line has  $m(\mathbf{r}) = 0.20$  ( $m(\mathbf{r}) = 0.01$ ).

We observed a huge structural change when the substitutional Mn is at the surface of the nanowire, at positions X and XI. The Mn atom makes a bond with the Ge second neighbor from the  $\{001\}$  and  $\{111\}$  faces for position X and XI respectively. The Mn atom becomes bonded to three Ge atoms and one H atom for position X and bonded to two Ge atoms and two H atoms for position XI. Consequently, there is a reaction with the formation of

an almost free-H<sub>2</sub> molecule. In this configuration, the impurity presented a lower formation energy, around 0.6 eV below site-I. This indicates that once Mn atoms are placed inside the NWs, there will be an energetic barrier opposing its migration towards the surface. However, for H-saturated wires, there might also be a large concentration of Mn atoms at the surface. We also looked for Mn at a tetrahedral interstitial site, because in the bulk the Mn at substitutional position has lower formation energy compared with interstitial one. The difference between the interstitial and substitutional formation energies in the center of the nanowire are 0.69 eV and 0.78 eV for diameters 27.0 Å and 18.7 Å respectively.

In figure 3 we show the net local magnetization for Mn,  $m(\mathbf{r}) = \rho_{up}(\mathbf{r}) - \rho_{down}(\mathbf{r})$ , a) at position I and b) Mn at position X. The behavior of the net local magnetization is highly localized around the Mn atom with an opposite magnetization that comes from  $p$ -states contribution from Ge nearest-neighbors, which is similar to what is observed for Mn in bulk<sup>20,21</sup>. The integrated value of  $m(\mathbf{r})$  is about  $3.00 \mu_B$  for all cases studied. The exception was for Mn at position VI where there is an increase of the magnetization to  $3.66 \mu_B$ .

In figure 4 we plot the Mn- $d$  partial spin density of states (PDOS), projected at the  $\Gamma$ -point, for the substitutional Mn atom at different sites in the GeNWs, (see figure 1). For all positions, similarly to Ge-bulk, the Mn atom introduces majority spin levels with strong  $d$  character and which are resonant with the valence band (VB). The highest occupied orbital (HOMO) and the lowest unoccupied orbital (LUMO) in the gap region have a strong  $p$ -character from Ge-atoms and a small  $d$ -component from Mn.

To understand the possibility of magnetic ordering, we studied the coupling between Mn-Mn atoms. We replaced two Ge-atoms by Mn and enforced different total spin configurations. For each of these Mn-pairs we computed the total energies for high spin state (ferromagnetic-FM) and low spin state (antiferromagnetic-AFM). Our simulation corresponds to a Mn concentration close to 2.0 %. We choose a few different pair configurations and the results are summarized in Table II. The notation in the first column of the table follow the labeled (I to XI) configurations presented in figure 1. The first two lines represent interactions between Mn oriented mostly along the longitudinal direction, whereas the others are interactions between Mn atoms positioned mostly along the same cross-section. For example, the I + VI Mn-Mn pair means one Mn atom at site I and another at site VI. In the second column we present the Mn-Mn distance. In the third column we show the total energy difference ( $\Delta E_f$ ) between the antiferromagnetic (AFM) and ferromagnetic

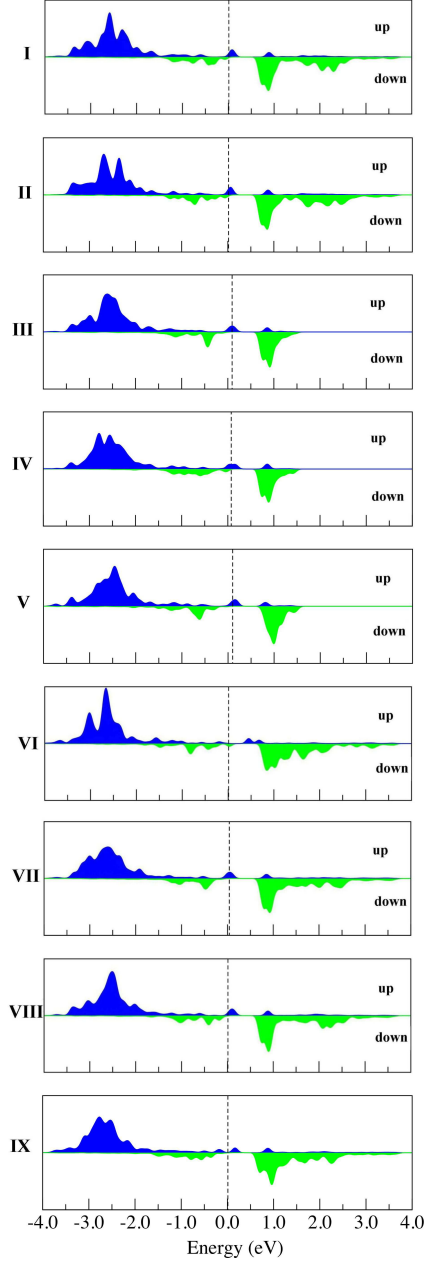


FIG. 4: (Color online) Mn impurity partial spin DOS, projected at the  $\Gamma$ -point, for Mn at different substitutional sites, (see figure 1). The dashed lines represent the Fermi energy.

(FM) ground states. The next two columns represent the local magnetic moments at each one of the Mn atoms where  $\mu_1(I)$  is the local magnetic moment for the Mn at position I and  $\mu_2$  represents the local magnetic moment for the second Mn atom. The last column gives the Mn-Mn direction. For the Mn atom at position I and another Mn as its first neighbor, we found an antiferromagnetic ground state with an energy difference  $\Delta E_f^{(AFM-FM)} = -0.69$  eV,



TABLE II: The magnetic coupling between Mn-Mn atoms. The first column represents the labeled (I to XI) configurations of figure 1. The  $d_{Mn-Mn}$  shows the distance between the two Mn atoms. The  $\Delta E_f^{(AFM-FM)}$  is the total energy difference between the AFM and FM states. The next two columns represent the local magnetic moment at each Mn atom. The last column gives the Mn-Mn direction. The first two lines represent interactions between Mn oriented mostly along the longitudinal direction, whereas the others are interactions between Mn atoms positioned mostly along the same cross-section.

Configuration	$d_{Mn-Mn}$ (Å)	$\Delta E_f^{(AFM-FM)}$ (eV)	$\mu_1$ (I) ( $\mu_B$ )	$\mu_2$ ( $\mu_B$ )	direction
I + I	4.07	0.22	3.48	3.48	[110]
I + I <sup>23</sup>	8.14	0.14	3.45	3.45	[110]
I + I <sup>st</sup>	2.00	-0.69	-2.87	2.87	$[\bar{1}\bar{1}\bar{1}]$
I + VIII	4.03	0.22	3.47	3.47	$[\bar{1}10]$
I + IV	4.79	0.12	3.50	3.46	$[3\bar{2}0]$
I + V	5.70	0.07	3.49	3.44	[001]
I + VII	7.13	0.07	3.52	3.44	$[\bar{3}62]$
I + VI	7.61	0.04	3.60	3.38	$[\bar{4}01]$
I + IX	8.33	0.10	3.42	3.54	$[\bar{1}10]$
I + X	8.89	0.00	3.16	3.46	$[\bar{6}2\bar{1}]$

as similarly to what has been observed in bulk calculations<sup>22</sup>. Position I + VII has a Mn-Mn distance smaller than position I + IX. However, the energy difference between AFM and FM states is slightly larger in I + IX. This is caused by variations of the coupling with the crystallographic directions<sup>21,24</sup>. For example, the I-IX Mn belong to the same Mn-Ge-Ge-Ge-Mn “zig-zag chain” perpendicular to the growth direction. For one Mn at position I, in the center, and another at position X, at the surface, with a large distance  $\sim 9$  Å, the high-spin and low-spin configurations are degenerate.

Comparing the results for different Mn-Mn distances in the GeNWs, see figure 5, we do not see an oscillatory AFM-FM behavior in the wire as has been observed for Ge-bulk<sup>22</sup>. We observe that for Mn-Mn distances ranging between 4.00 Å to 8.00 Å the ferromagnetic coupling is very similar.

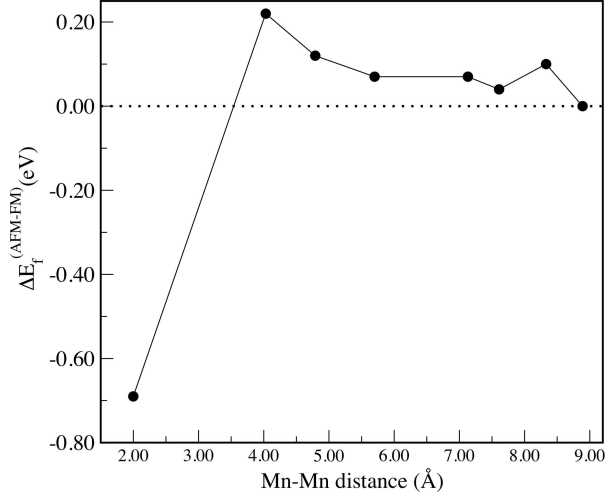


FIG. 5: Total energy difference between AFM and FM states, for Mn-Mn coupling as a function of the Mn-Mn distance. They correspond to the last eight lines in table II. The dashed line is only guides to the eye.

In figure 6 we show, for two Mn atoms as first neighbors, the local magnetization,  $m(\mathbf{r}) = \rho_{up}(\mathbf{r}) - \rho_{down}(\mathbf{r})$ , and its contour plots (in  $e/\text{\AA}^3$ ). The cross-sectional plane passes through the Mn atoms. The Mn atoms are with spin flipped (a) and (b), and aligned (c) and (d). The most stable configuration, for this position, is an antiferromagnetic state, (a) and (b), with Mn-Mn distance equal 2.00 Å. This small distance between Mn atoms lead to a direct overlap and consequently to an increase of the energy of the FM state when compared to AFM configuration due to the Pauli exclusion principle.

#### IV. CONCLUSION

In summary, we have performed a systematic study, using total energy *ab initio* calculations, of the electronic and magnetic properties of Mn doped Ge nanowire. Our results show that Mn has lower formation energy at the center position of the GeNWs when compared to regions close to the surface. This indicates that once Mn atoms are placed inside the NWs, there will be an energetic barrier opposing its migration towards the surface. However, if the NWs are saturated with H atoms, we expect a large concentration of Mn atoms at the surface, where the formation energy is lower than at the center of the wire by 0.6 eV. The Mn impurity introduces a local magnetic moment due to *d*-levels resonant with the VB. The

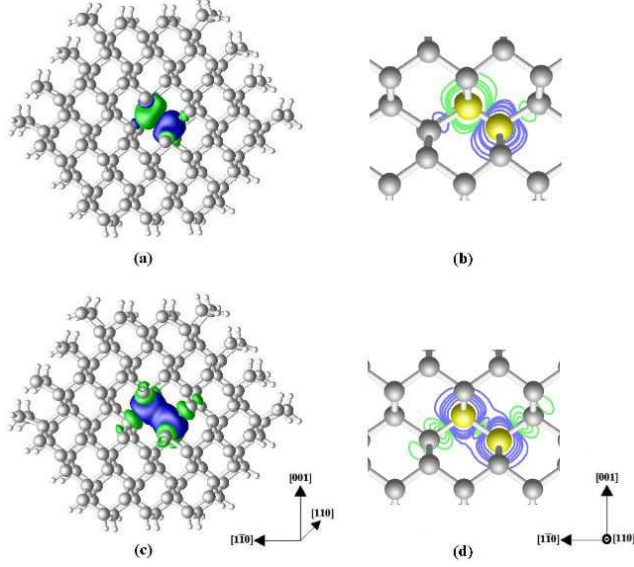


FIG. 6: (Color online) Isosurfaces for the local magnetization  $m(\mathbf{r}) = \rho_{up}(\mathbf{r}) - \rho_{down}(\mathbf{r})$  for two Mn atoms, one at position I and another as its first neighbor. The small spheres represent the hydrogen atoms, the gray ones represent the Ge atoms and the yellow (large) spheres represent the Mn atoms. Blue (green) regions show predominant  $\rho_{up}$  ( $\rho_{down}$ ) electronic densities. The more spherical isosurfaces correspond to a net spin value of  $+0.01e/\text{\AA}^3$  (blue) and  $-0.01e/\text{\AA}^3$  (green). In (a) and (b) we present an AFM state and in (c) and (d) a FM state. The most stable configuration, for this position, is an antiferromagnetic state. In (b) and (d) we show the contour plots (in  $e/\text{\AA}^3$ ) for the local magnetization at a plane, that passes through the Mn atoms. The green lines correspond to the isosurfaces -0.01, -0.03, -0.05, -0.07 and -0.09, whereas the blue ones correspond to the values 0.01, 0.03, 0.05, 0.07 and 0.09.

Mn-Mn coupling is always ferromagnetic except for first neighbor configurations.

We acknowledge support from the Brazilian agencies FAPESP and CNPq and the computational facilities of the Centro Nacional de Processamento de Alto Desempenho (CENAPAD-Campinas). We thank Dr. G. M. Dalpian for useful discussions.

---

<sup>1</sup> D. J. Sirbuly, M. Law, H. Yan, and P. Yang, J. Phys. Chem. B **109**, 15190 (2005).

<sup>2</sup> Y. Wu, Y. Cui, L. Huynh, C. J. Barrelet, D. C. Bell, and C. M. Lieber, Nano Lett. **4**, 433 (2004).

- <sup>3</sup> L. J. Lauhon, M. S. Gudixsen, D. Wang, and C. M. Lieber, *Nature* **420**, 57 (2002).
- <sup>4</sup> I. Žutić, J. Fabian, and S. Das Sarma, *Rev. Mod. Phys.* **76**, 323 (2004).
- <sup>5</sup> A. H. MacDonald, P. Schiffer, and N. Samarth, *Nature Mat.* **3**, 195 (2005).
- <sup>6</sup> Y. D. Park, A. T. Hanbicki, S. C. Erwin, C. S. Hellberg, J. M. Sullivan, J. E. Mattson, T. F. Ambrose, A. Wilson, G. Spanos, and B. T. Jonker, *Science* **295**, 651(2002).
- <sup>7</sup> S. Cho, S. Choi, S. C. Hong, Y. Kim, J. B. Ketterson, Bong-Jun Kim, Y. C. Kim, and Jung-Hyun Jung *Phys. Rev. B* **66**, 033303 (2002).
- <sup>8</sup> M. Bolduc, C. Awo-Affouda, A. Stollenwerk, M. B. Huang, F. Ramos, and V. P. LaBella, *Nucl. Instr. and Meth. B* **242**, 367 (2006).
- <sup>9</sup> A. J. R. da Silva, A. Fazzio, and A. Antonelli, *Phys. Rev. B* **70**, 193205 (2004).
- <sup>10</sup> H. Nakashima, and K. Hashimoto, *J. Appl. Phys.* **69**, 1440 (1991).
- <sup>11</sup> P. Poddar, Y. Sahoo, H. Srikanth, and P. N. Prasad, *Appl. Phys. Lett.* **87**, 062506 (2005).
- <sup>12</sup> T. M. Schmidt, P. Venezuela, J. T. Arantes, and A. Fazzio, *Phys. Rev. B* **73**, 235330 (2006).
- <sup>13</sup> X. Huang, A. Makmal, J. R. Chelikowsky and L. Kronik, *Phys. Rev. Lett.* **94**, 236801 (2005).
- <sup>14</sup> P. V. Radovanovic, C. J. Barrelet, S. Gradec, F. Qian, and C. M. Lieber, *Nano Lett.* **5**, 1407 (2005).
- <sup>15</sup> J. P. Perdew and Y. Wang, *Phys. Rev. B* **45**, 13244(1992).
- <sup>16</sup> D. Vanderbilt, *Phys. Rev. B* **41**, 7892(1990).
- <sup>17</sup> G. Kresse and J. Hafner, *Phys. Rev. B* **47**, R558 (1993); G. Kresse and J. Furthmüller, *ibid.* **54**, 11169 (1996).
- <sup>18</sup> T. Hanrath and B. A. Korgel, *Small* **1**, 717(2005).
- <sup>19</sup> First-principles DFT calculations always underestimate the band gap energy. In fact, results for Si nanowires show that a GW correction is important to determine the correct band gap: X. Zhao, C. M. Wei, L. Yang, and M. Y. Chou, *Phys. Rev. Lett.* **92**, 236805 (2004).
- <sup>20</sup> G. M. Dalpian, Antônio J. R. da Silva, and A. Fazzio, *Phys. Rev. B* **68**, 113310 (2003).
- <sup>21</sup> Antônio J. R. da Silva, A. Fazzio, R.R. dos Santos and L.E. Oliveira, *Phys. Rev. B* **72**, 125208 (2005); *J. Phys.: Condens. Matter* **16**, 8243 (2004).
- <sup>22</sup> A. Stroppa, S. Picozzi, A. Continenza and A. J. Freeman, *Phys. Rev. B* **68**, 155203 (2003).
- <sup>23</sup> For this Mn-Mn distance we use a doubled cell with diameter  $d \simeq 27.0 \text{ \AA}$  described in the calculation procedure with a Brillouin zone sampling at the  $\Gamma$ -point.
- <sup>24</sup> Y. -J. Zhao, P. Mahadevan and A. Zunger, *J. Appl. Phys.* **98**, 113901 (2005).